
This is an electronic reprint of the original article.
This reprint may differ from the original in pagination and typographic detail.

Ding, Er Xiong; Liu, Peng; Khan, Abu Taher; Zhang, Qiang; Wei, Nan; Jiang, Hua; Kauppinen, Esko I.

Towards the synthesis of semiconducting single-walled carbon nanotubes by floating-catalyst chemical vapor deposition

Published in:
Carbon

DOI:
[10.1016/j.carbon.2022.04.020](https://doi.org/10.1016/j.carbon.2022.04.020)

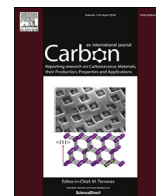
Published: 15/08/2022

Document Version
Publisher's PDF, also known as Version of record

Published under the following license:
CC BY

Please cite the original version:
Ding, E. X., Liu, P., Khan, A. T., Zhang, Q., Wei, N., Jiang, H., & Kauppinen, E. I. (2022). Towards the synthesis of semiconducting single-walled carbon nanotubes by floating-catalyst chemical vapor deposition: Challenges of reproducibility. *Carbon*, 195, 92-100. <https://doi.org/10.1016/j.carbon.2022.04.020>

This material is protected by copyright and other intellectual property rights, and duplication or sale of all or part of any of the repository collections is not permitted, except that material may be duplicated by you for your research use or educational purposes in electronic or print form. You must obtain permission for any other use. Electronic or print copies may not be offered, whether for sale or otherwise to anyone who is not an authorised user.



Towards the synthesis of semiconducting single-walled carbon nanotubes by floating-catalyst chemical vapor deposition: Challenges of reproducibility



Er-Xiong Ding¹, Peng Liu¹, Abu Taher Khan¹, Qiang Zhang^{*}, Nan Wei, Hua Jiang, Esko I. Kauppinen^{**}

Department of Applied Physics, Aalto University School of Science, Puumiehenkuja 2, 00076, Aalto, Espoo, Finland

ARTICLE INFO

Article history:

Received 3 February 2022
Received in revised form
18 March 2022
Accepted 6 April 2022
Available online 8 April 2022

Keywords:

Gas-phase synthesis
Semiconducting single-walled carbon nanotubes
Pressure
Methanol
Reproducibility

ABSTRACT

High-purity semiconducting single-walled carbon nanotubes (s-SWCNTs) are of paramount significance for the fabrication of high-performance electronics. Here, we present continuous production of high-purity, long, and isolated s-SWCNTs by gas-phase synthesis, retaining the pristine morphologies of as-synthesized nanotubes. The s-SWCNTs were synthesized at *ca.* 920 °C using ethanol and methanol as carbon source and growth enhancer, respectively in N₂ and H₂. The purity of as-produced s-SWCNTs with a mean length of 15.2 μm can reach 98% as determined by optical absorption spectroscopy. We observed that the overpressure in the reactor and methanol are the principal causes of the enrichment of s-SWCNTs. Specifically, the s-SWCNTs were found to be more negatively charged, and oxygen-contained species play critical roles in the s-SWCNT synthesis. Through the demonstration of field-effect transistors, the s-SWCNTs exhibit a high mean charge carrier mobility of 453.3 cm² V⁻¹ s⁻¹ which is 2.27 times higher than that of the transistors fabricated with high-quality dispersion-processed SWCNTs. Additionally, we discuss the challenges of synthesis repeatability and recommend a few tips to improve reproducibility. Our study represents an important step towards the scalable production of clean, long, and isolated s-SWCNTs with high purity and narrow bandgap distribution.

© 2022 The Author(s). Published by Elsevier Ltd. This is an open access article under the CC BY license (<http://creativecommons.org/licenses/by/4.0/>).

1. Introduction

Single-walled carbon nanotubes (SWCNTs) have been considered as promising candidates for constructing next-generation electronics because of their exceptional electrical and optical properties [1–3]. Semiconducting SWCNTs (s-SWCNTs) are aggressively applied in the semiconductor field in, *e.g.*, digital electronics [4], thermoelectric generators [5], and photovoltaics [6]. For instance, a transistor employing s-SWCNTs as a channel material simultaneously exhibits a superior on/off current ratio and excellent charge carrier mobility [7], compared to transistors using organic semiconductors as the channel material [8]. The scalable production of highly enriched s-SWCNTs is, thus, imperative for

their large-scale applications.

High-purity s-SWCNTs can be separated from raw SWCNT powder dispersed in a solvent via well-established methods like density gradient ultracentrifugation [9], gel chromatography [10], or polymer-assisted extraction [11]. Substrate chemical vapor deposition (CVD) growth [12] and selective etching of metallic SWCNTs (*m*-SWCNTs) [13] are also general techniques to produce high-purity s-SWCNTs. Nevertheless, ultrahigh-performance devices utilizing those s-SWCNTs have faced several obstacles. Dispersion-sorted s-SWCNTs undergo repeated intense sonication, during which nanotubes become damaged and dirty (covered by residual dispersant) [14]. The introduced structural defects are unlikely to get repaired and contaminants are difficult to remove. These introduced imperfections in turn deteriorate the performance of CNT transistors [15]. The typical mean length of dispersion-sorted s-SWCNTs is below ~2 μm [16,17], which is one of the limiting factors to their applications in high-performance thin-film transistors. CVD-grown s-SWCNTs on a substrate suffer from low yield, which is limited by the number of active catalyst

^{*} Corresponding author.

^{**} Corresponding author.

E-mail addresses: qiang.zhang@aalto.fi (Q. Zhang), esko.kauppinen@aalto.fi (E.I. Kauppinen).

¹ E.-X. Ding, P. Liu, and A.T. Khan contributed equally to this work.

particles immobilized on the substrate [14], preventing them from being applied at a pilot scale. Additionally, as-grown *s*-SWCNTs have to be transferred by some binder, e.g., poly(methyl methacrylate), to a temperature-sensitive substrate for flexible and/or stretchable device applications, which readily introduces impurities into the nanotubes [18]. Consequently, a facile process for the scalable production of high-quality *s*-SWCNTs would be highly appreciated.

To meet this end, we have developed a single-step process for the continuous production of high-purity *s*-SWCNTs in a floating catalyst CVD (FCCVD) reactor (Fig. S1), which enables us to fabricate tunable-density *s*-SWCNT networks retaining their pristine morphologies onto any substrate. With the FCCVD technique, O₂ [19,20] or H₂ [21] was introduced into the reactor as an *in-situ* etchant for the synthesis of *s*-SWCNTs, though the electrical quality of the *s*-SWCNTs needs to be further improved for ultrahigh performance electronics. We reported the purity of 76.8% of *s*-SWCNTs in our previous work using ethanol as the carbon source [22]. It was suggested that methanol, as a weak etchant, has the potential to enrich *s*-SWCNTs by preferentially etching some *m*-SWCNTs with substrate CVD [23]. Hence, ethanol and methanol were selected as the carbon source and growth enhancer, respectively, for *s*-SWCNT synthesis in this work. The impacts of the barometric pressure (relative gas pressure used in this work) inside the synthesis reaction system and methanol concentration on *s*-SWCNT purity were investigated through optical and microscopic characterizations. *In-situ* Fourier-transform infrared (FT-IR) spectrometer and aerosol electrometer were applied to monitor CNT synthesis. Then, field-effect transistors (FETs) were fabricated to examine the electrical performance of as-synthesized *s*-SWCNTs. We also tried to reproduce high-purity *s*-SWCNTs and provide some suggestions to improve the process reproducibility.

2. Experimental

2.1. Synthesis of *s*-SWCNTs

Ethanol (99.5%, Altia Oyj, Finland) is the carbon source, ferrocene (98%, Sigma-Aldrich) and thiophene ($\geq 99\%$, Sigma-Aldrich) were utilized as catalyst and promoter precursors, respectively. A variable volume (0–40 v%) of methanol (99.9%, Acros Organics) was intentionally added to enhance the growth of *s*-SWCNTs. Ethanol solution containing methanol, 0.25 wt% ferrocene, and a small amount of thiophene (molar ratio of sulfur to iron is in the range of 0.125–0.175) was sonicated for 1 min in a vial to form a homogeneous solution which was injected into a heating line using a syringe pump (NE-1000 series, New Era Pump Systems, USA) at a feeding rate of 1–4 $\mu\text{l}/\text{min}$. The evaporated precursors in the heating line at 130 °C were carried by 300 standard cubic centimeters (sccm) N₂ (vaporized from liquid nitrogen supplied by AGA, Finland, and purified by an oxygen/moisture trap, OT3-4, Agilent) and 7.5–26 sccm H₂ (99.999%, AGA, Finland). The reactor temperature for SWCNT synthesis was adjusted in the range of 900–940 °C. As-produced SWCNTs were collected at the reactor outlet using a patterned $\phi 25$ mm membrane filter (the effective collection area was scaled to ca. 5×5 mm² through patterning). The barometric pressure inside the quartz tube was raised due to the usage of a patterned filter. The samples were collected with a 250 sccm vacuum from a 320 sccm total gas flow, exhausting the surplus gas via the bypass line. The collection time for a 5×5 mm² film with a transmittance (T) of ca. 95% was around 1–2 h. The pressure (0–20 kPa) inside the quartz tube was regulated with a needle valve (to partially block the exhaust) mounted at the reactor outlet and was measured with a precision digital test gauge (type 2084, Ashcroft, USA).

2.2. Characterizations of *s*-SWCNTs

For optical characterizations, the films on membrane filters were press-transferred onto quartz slides ($35 \times 20 \times 1$ mm³, HSQ300, FinnishSpecialGlass Oy, Finland). A UV–Vis–NIR spectrometer (Agilent Cary 5000) was utilized to record the optical absorption spectrum in the range of 200–2500 nm. The data interval was set to be 1 nm to acquire the fine features of the absorption spectrum. The baseline was subtracted before each measurement by placing one clean quartz slide in the reference beam path and another in the sample beam path. The purity of *s*-SWCNTs was calculated from the absorption spectrum, and the calculation methods are described in Fig. S2. Based on the absorption spectrum, SWCNT diameter distribution was fitted with a Matlab code [24]. FT-IR spectra were acquired with a Nicolet Antaris IGS analyzer. Raman spectra were collected using a Raman spectrometer (Horiba Jobin-Yvon Labram HR 800) equipped with four excitation wavelengths, i.e., 488 nm, 514 nm, 633 nm, and 785 nm. Each present Raman spectrum was averaged from three spectra taken at different locations on the film (the distance between successive measurements was set to be 50 μm to avoid multiple detections of the same nanotube). A suitable filter size was selected to reduce the laser intensity to avoid beam damage to SWCNTs. An Aerosol Electrometer 3068B was employed to detect the total net current of the products from the reactor exhaust. For length measurement, sparsely distributed SWCNTs were deposited onto a SiO₂/Si substrate via a thermophoretic method [25] for imaging with a scanning electron microscope (SEM, Zeiss Sigma VP). A JEOL 2200FS Double Cs-corrected transmission electron microscope (TEM) operated at 80 kV was employed to gather the electron diffraction patterns of the SWCNTs deposited onto a copper grid coated with lacey carbon film. SWCNT chiralities were determined from their electron diffraction patterns using the intrinsic-layer-line spacing method [26].

2.3. Fabrication of FETs

A fast and ultraclean approach [27] was adopted to fabricate and characterize devices. Conventional photolithography and lift-off processes were employed to fabricate bottom gate FETs. The backside of the boron-doped p⁺⁺ silicon wafer (Electrokem Oy) functions as the gate and the thermally grown oxide layer (100 nm thick) performs as an insulating layer between the metal contact and silicon. Conventional photolithography (Süss Microtec MA6/BA6) and electron beam evaporator were utilized to pattern electrodes using Ti/Pd with a thickness of 5 nm/25 nm. Then, the as-produced SWCNTs were deposited onto pre-fabricated arrays of contacts with a thermophoretic deposition method [25]. Before electrical characterization, the chips were annealed at ambient at 200 °C for 2 h. The electrical characterization was performed at ambient and at room temperature utilizing an automated probe station (PA200, SUSSMicroTec AG, Germany) with the combination of a semiconductor parameter analyzer (Agilent 4168, USA).

3. Results and discussion

3.1. Synthesis of highly enriched *s*-SWCNTs

Initial optimization of the growth parameters to obtain high-purity *s*-SWCNTs was based on the analyses of optical absorption spectra. To minimize the influence of ambient doping on *s*-SWCNTs, all the absorption spectra were acquired immediately upon extracting the film sample from the reactor downstream (air exposure time throughout the whole process was approximately 2 min). During the optimization period, we found that the

barometric pressure inside the quartz tube significantly affected the heights and widths of the characteristic peaks of the absorption spectrum, *i.e.*, the first and second interband transitions of semi-conducting nanotubes (E_{11}^S and E_{22}^S), and the first interband transition of their metallic counterparts (E_{11}^M). The atmospheric pressure inside the reaction tube produced low, wide S_{11} and S_{22} peaks (*i.e.*, 0 kPa in Fig. 1a), indicating a broad diameter distribution of as-synthesized SWCNTs. In contrast, SWCNTs produced at a slight overpressure (caused by the partial blockage of the exhaust) generated higher, narrower S_{11} and S_{22} peaks (Fig. 1a), reflecting their narrower diameter distribution. Further increases in pressure moderately elevated the height of S_{11} peak and the purity of s-SWCNTs (Fig. 1b). The purity of s-SWCNTs is the highest when the overpressure of 14 kPa was set. Raman analysis supported our findings on the effect of pressure on s-SWCNT purity. Radial breathing mode (RBM) peaks excited by 488 nm (Figs. 1c) and 514 nm (Fig. 1d) lasers indicate that some small-diameter *m*-SWCNTs are present in the sample collected at 0 kPa. Some *m*-SWCNTs in each sample were resonant with a 633 nm laser, but their proportion is the lowest in the sample collected at 14 kPa (Fig. 1e). The barometric pressure inside a quartz tube was found to be able to modulate the purity of as-synthesized s-SWCNTs. We hypothesize that this arises because overpressure promotes the growth of s-SWCNTs with specific chiral indices by lowering their nucleation barriers and accelerating the formation of corresponding carbon caps [28], or by producing catalyst particles with more even morphology and/or structure distribution [29,30]. Theoretical calculations have predicted that large-chiral angle SWCNTs need lower activation energies for cap formation compared to those with smaller chiral angles [31,32]. It has also been reported that higher pressure inside the reaction system favors the growth of SWCNTs with specific chiral indices, narrowing either the chirality distribution [28] or the diameter distribution [33]. In this work, a few low absorption peaks can be found in the S_{11} region of the spectrum labeled with 0 kPa. Whereas other spectra present a sharp and dominant peak in the S_{11} region while the neighboring absorption peaks are suppressed, revealing the enrichment of s-SWCNTs with

certain chiral indices and narrow chirality distributions. Additionally, the SWCNT diameter distributions fitted from the absorption spectra show that ~55% of the nanotubes collected at 20 kPa have diameters in the range of 1.2–1.4 nm, and the proportion is nearly twice that (~28%) of the nanotubes collected at 0 kPa (Fig. S3).

We also noticed that the heights of the characteristic peaks in the absorption spectra are sensitive to the concentration of methanol in the precursor solution. It is worth noting that S_{11} height, relative to that of the π plasmon peak, rises with increasing methanol concentration, implying the increased population of specific chiral indices and the shrinkage in diameter distributions. The purity of the s-SWCNTs synthesized without methanol is lower than that obtained with the addition of a suitable amount of methanol, although an excess of methanol again decreases the purity (Fig. 2a, Fig. S5). The fitted diameter distribution (based on the absorption spectrum) of the SWCNTs synthesized with the addition of 18 v% methanol demonstrates an increased proportion of diameters in the range of 1.2–1.4 nm (Fig. S6c), which verifies the results obtained from the absorption spectra. The intensity reductions in some of the high-frequency RBM peaks in the Raman spectra of the SWCNTs synthesized with high methanol concentrations reveal the reduction or absence of some zigzag and near-zigzag nanotubes (Fig. S7), which is in accordance with the reduced percentage of narrow-diameter SWCNTs (Fig. S6). However, the mean diameter of the SWCNTs collected with 18 v% methanol modestly increased to *ca.* 1.31 nm from *ca.* 1.29 nm when no methanol was added (Figs. S6a and c). One explanation for the methanol effect observed here can be the selective etching of *m*-SWCNTs by the oxygen-containing group [23,34,35]. When a proper volume of methanol is added, the oxygen-containing radicals decomposed from ethanol and methanol can selectively etch some *m*-SWCNTs, which have lower ionization energy and are more reactive [23,36,37], resulting in the enrichment of s-SWCNTs. Further addition of methanol into the precursor solution could, however, induce the etching of both *m*-SWCNTs and narrow-diameter s-SWCNTs with higher curvatures [38]. We have found that when the methanol concentration surpass 50 v%, the collection

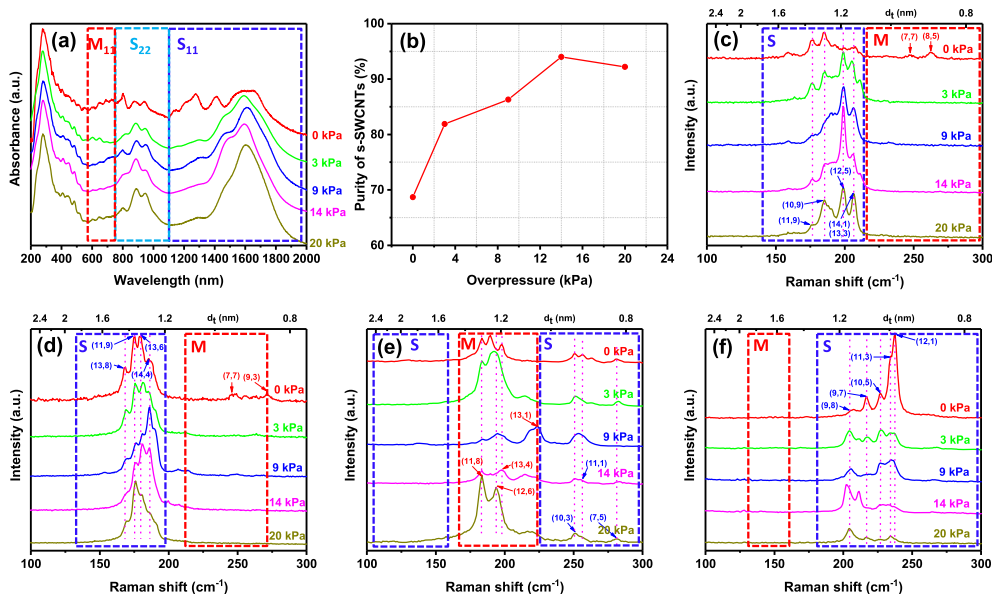


Fig. 1. Optical characterizations of the effect of barometric pressure inside the quartz tube on the purity of s-SWCNTs. (a) Absorption spectra of SWCNTs collected at different pressures. (b) Calculated purities of s-SWCNTs from the corresponding spectra displayed in (a). The calculation method of s-SWCNT purity can be found in Fig. S2. (c)–(f) are RBM regions in Raman spectra of SWCNTs resonant with laser wavelengths of 488 nm, 514 nm, 633 nm, and 785 nm, respectively. S and M refer to s-SWCNTs and *m*-SWCNTs, respectively. The labeled numbers are the chiral indices of SWCNTs. 940 °C–22 sccm H₂–14 v% methanol. (A colour version of this figure can be viewed online.)

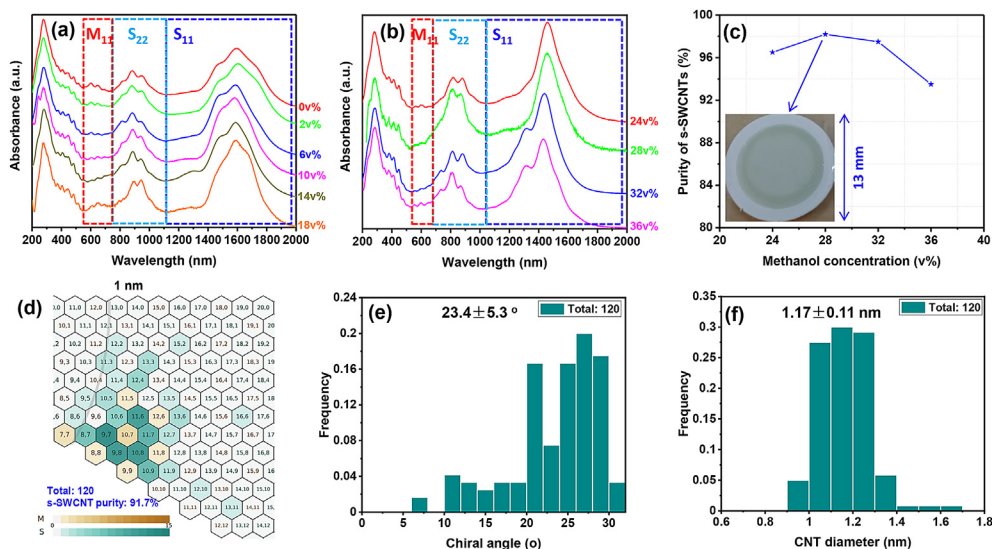


Fig. 2. Optical absorption analysis of the effect of methanol concentration on the purity of s-SWCNTs and electron diffraction results. (a) and (b) are absorption spectra of the SWCNTs synthesized with low and high methanol concentrations, respectively. Parameters for (a) are 940 °C-22 sccm H₂-14 kPa, for (b) are 920 °C-7.5 sccm H₂-14 kPa. (c) Calculated purities of s-SWCNTs from the corresponding spectra in (b). The inserted photograph is a light green semiconducting-enriched SWCNT film on a membrane filter ($\phi = 13$ mm), demonstrating the ability of our reactor for the scalable production of s-SWCNTs. (d) Chirality map of SWCNTs, showing an s-SWCNT purity of 91.7%. The number in a hexagon refers to the chiral index, (n,m) of an SWCNT. M and S in the profile represent metallic and semiconducting SWCNTs, respectively. 920 °C-7.5 sccm H₂-14 kPa-28 v%. (e) and (f) are chiral angle and diameter distributions, respectively, extracted from the map in (d). (A colour version of this figure can be viewed online.)

time of a 90° T film was greatly increased. The decreased yield of SWCNTs at high methanol concentrations might indirectly support the etching proposal.

To further increase the purity of s-SWCNTs, we moderately adjusted other growth parameters. Through slight tuning of growth temperature and H₂ flow rate, we noticed that more s-SWCNTs were produced at a lower temperature and a reduced H₂ flow rate (Fig. S9). Decreasing the flow rate of H₂ leads to a blueshift of S₁₁ in the absorption spectrum (Fig. S9b), indicating a reduction in SWCNT mean diameter. As can be observed from the fitted diameter distributions (Fig. S10), the mean diameter of SWCNTs decreased to ca. 1.23 nm from ca. 1.29 nm when the H₂ flow rate was reduced to 7.5 sccm from 18 sccm. The enhanced growth of narrow-diameter SWCNTs at a lower H₂ flow rate may be attributed to fewer carbon radicals being decomposed from ethanol via hydrogen abstraction [41]. The modulation of SWCNT mean diameter by H₂ has also been reported elsewhere [22]. An optimal combination of growth parameters was then identified and s-SWCNTs with a purity close to 98% were produced (Fig. 2b and c). It should be noted that far fewer m-SWCNTs in the 28 v% methanol sample were resonant at the excitation wavelength of 633 nm (Fig. S12c). The purity of s-SWCNTs varied slightly in the optimum window of methanol concentration, then began to decline when excessive methanol was added (Fig. 2b and c). In contrast to the variation tendency of SWCNT mean diameter at low methanol concentrations (Fig. S6), the SWCNT mean diameter obtained at a high methanol concentration regime was reduced to ca. 1.12 nm from ca. 1.23 nm with increasing methanol amount (Fig. S11). RBM peaks also show a growing number of narrow-diameter SWCNTs with increasing methanol concentration (Fig. S12). The presence of more narrow-diameter SWCNTs at an increased methanol concentration is ascribed to a higher proportion of small-sized catalyst particles. The scenario might be similar to the impediment of catalyst from Ostwald ripening via hydroxyl stabilization of the nanoparticles on a substrate [42]. It is also possible that the active area of catalyst particles is shrinking with methanol concentration, due to partial oxidation of particles by oxygen-containing groups from methanol. Additionally, we would like to emphasize that the

as-synthesized SWCNTs possess superior structural quality, which is supported by the high peak ratios of graphitic (G) and disorder-induced (D) bands in the Raman spectra (Fig. S4, S8, S13).

In order to unambiguously determine the chiral indices of SWCNTs and s-SWCNT purity, individual SWCNTs were probed for their electron diffraction patterns (Fig. S14). We selected the parameter of methanol concentration here to examine the purity of s-SWCNTs with electron diffraction and to validate the etching behavior proposed in the literature [23,34,35]. The chirality map of SWCNTs synthesized with 28 v% methanol presents more clustered chiral indices than that obtained without methanol addition, although their mean chiral angles and mean diameters are similar (Fig. 2d–f, Fig. S15). The purity of s-SWCNTs produced with the addition of 28 v% methanol was determined to be 91.7% by electron diffraction (Fig. 2d), which is ~5% lower than the purity of ~97% calculated from the absorption spectrum (Fig. S18). This discrepancy may arise from the distinction between absorption and limited-counting-based characterizations, provided that s-SWCNTs are longer than the metallic counterparts [43]. Zhang et al. [29] also found a difference of 3% between the purities of s-SWCNTs determined by absorption and electron diffraction. Additionally, the gatherings of the chiral indices (9,7), (10,8), and (9,8) (Fig. S17), and the narrow diameter distribution (87% of nanotube diameters are in the range of 1.0–1.3 nm, Fig. 2f) are deemed to be responsible for the appearance of sharp and high S₁₁ peak displayed in Fig. S18. Based on the chirality distribution in the maps, selective etching of m-SWCNTs by oxygen-containing chemicals contributed by methanol could be one of the causes of the enrichment of s-SWCNTs, which is supported by Raman analysis and mechanism investigation described below.

Prior to the electrical characterization, we measured the lengths of as-synthesized SWCNTs deposited onto a silicon substrate (Fig. S19a). The mean bundle length of the SWCNTs collected under optimized conditions is 15.2 μ m (standard deviation is 9.4 μ m) (Fig. S19b), which is only half that reported in our previous studies without the addition of methanol [22,44]. The as-produced SWCNTs are highly isolated due to the low number concentration (Fig. S19c). SWCNT bundles with lengths shorter than 5 μ m account

for ~14% of the total, while the corresponding fraction is less than 1% in our previous work [44], which also suggests the etching role of oxygen-containing radicals decomposed from methanol.

To evaluate the electrical performance of s-SWCNTs, we characterized the FETs incorporating as-produced SWCNTs. The FET chips were fabricated using a common bottom gate design, with a channel length of 2 μm and width of 5 μm [27]. A working FET is considered as semiconducting if the ratio of on-current to off-current ($I_{\text{on}}/I_{\text{off}}$) is above 100. 37% of the devices among the working ones turn out to be metallic (Fig. S20). We attribute this phenomenon to two factors. First, some devices have more than one SWCNT bridging the channel. Second, because the SWCNTs in this study are considerably longer than our previous studies, some SWCNTs are bridging the neighboring devices. These factors contribute to the larger fraction of metallic devices and cannot be easily modeled. Therefore, we only utilized the devices to show that the SWCNTs are of high electrical quality by picking out the single-SWCNT bundle devices upon SEM inspection. In order to obtain highly enriched semiconducting devices, further modification of the chip design (e.g., large distance between two pairs of electrodes), fine-tuning of SWCNT density (e.g., low density), and careful characterization (e.g., long integration time) of FETs are needed, which we consider as future work. The charge carrier mobility (μ_{FE}), on-state current (I_{on}), and off-state current (I_{off}) ratio were extracted to assess the electrical quality of the s-SWCNTs. The peak transconductance formula was used to extract the charge carrier mobility (μ_{FE}) of semiconducting device. To investigate the charge transfer properties of s-SWCNTs, we selected 20 semiconducting devices that exhibited good on-state conductance ($G_{\text{on}} = I_{\text{d}}/V_{\text{ds}}$). Fig. 3a displays transfer characteristics of the 20 FETs, with semiconducting behavior, exhibiting clear p-type characteristics. The mean μ_{FE} value of the 20 FETs is $453.3 \pm 98.8 \text{ cm}^2 \text{ V}^{-1} \text{ s}^{-1}$ (Fig. 3b), suggesting superior transport properties of s-SWCNTs. The mean μ_{FE} is 2.27 times higher than that ($200 \text{ cm}^2 \text{ V}^{-1} \text{ s}^{-1}$) of high-quality dispersion-processed SWCNT-based transistors measured using a similar method [45]. The mean value of $I_{\text{on}}/I_{\text{off}}$ of the 20 FETs is 2.43×10^7 (Fig. S21), indicating excellent switching efficiency of the s-SWCNT FETs. In addition, the devices exhibit G_{on} with a mean value of 2.85 μS at $V_{\text{ds}} = -2 \text{ V}$. The exceptional performance of SWCNT-based FETs, demonstrated by high values of μ_{FE} and $I_{\text{on}}/I_{\text{off}}$, reflects the high quality of these as-synthesized s-SWCNTs for electronics.

3.2. s-SWCNTs with moderate purities

As we found the conditions for the scalable growth of highly enriched s-SWCNTs which are extremely useful for large-scale optoelectronics, we have been aiming to reproduce s-SWCNTs

with the same purities. For some unknown reasons, we could not reproduce s-SWCNTs with a purity close to 95% (calculated from optical absorption spectrum) for the moment, though we still would like to share our progress. We believe that there exists some certain parameter combination or a sweet window where highly enriched s-SWCNTs could be synthesized with our reactor. Nevertheless, we successfully found that the effects of methanol concentration and H_2 flow rate are consistent with the tendency displayed in Figs. 1 and 2. As presented in Fig. 4a, c, the purity of s-SWCNTs gradually increases first then decreases sharply with increasing the concentration of methanol. H_2 with a lower flow rate of 7.5 sccm narrows SWCNT diameters and their distributions, resulting in a higher purity of s-SWCNTs (Fig. 4b, d). However, adjusting the pressure inside the quartz tube induces negligible changes in the purity of s-SWCNTs (Figs. S22a and b).

Then, to explore the mystery behind the variation in the purity of s-SWCNTs, we utilized a gas-phase FT-IR spectrometer and an aerosol electrometer for *in-situ* monitoring of as-synthesized SWCNTs. The IR results suggest that CO and CH_4 are the main direct carbon sources for the growth of SWCNTs. High-chiral angle SWCNTs which require low activation energy for cap formation could preferably grow in an enriched CO atmosphere when the concentration of methanol is increased [31,32,46] (Fig. 5a). In addition, the amount of H_2O is very sensitive to the variation of methanol concentration. The H_2O concentration has a dramatic rise of 125 ppm when the methanol concentration increases to 28 v% from 0 v% (Fig. 5a), indicating that the decomposed H_2O could etch the unstable *m*-SWCNTs when an appropriate amount of methanol is added [47,48]. It should be noted that other possible mechanisms of the enrichment of s-SWCNTs can not be simply excluded. It has been proposed that H_2O can modify the structure and/or morphology of catalyst particle [39,40], and can affect the nucleation of SWCNTs [12]. The shaping of particle morphology by H_2O can also account for the narrowed mean diameter of SWCNTs when the methanol concentration is increased (Fig. S11), which has been mentioned above. Thus, the enrichment of s-SWCNTs in this work could be realized through the synergistic effects of etching, nanoparticle reshaping, and selective nucleation. Induced by the chemical equilibrium, one aspect of Le Chatelier's principle, the reverse reaction of ethanol and methanol decomposition enhances as the pressure inside the system increases, which is confirmed by the reduced carbon source concentration at elevated pressure (Fig. S22c). Whereas the H_2O concentration only has a moderate increase (less than 50 ppm) with pressure.

An aerosol electrometer was employed to monitor the total net current of as-produced gas-phase SWCNTs. The experimental results indicate that the net charge of the SWCNTs produced in the ethanol-based system is negative in this work. The measured

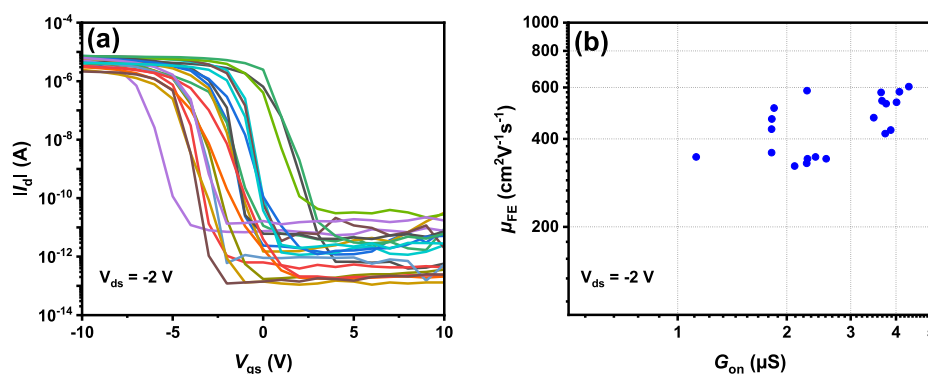


Fig. 3. Electrical characterization of SWCNT-FETs. (a) Transfer characteristics ($I_{\text{d}} - V_{\text{gs}}$) of 20 semiconducting devices with gate sweeping (V_{gs}) from -10 V to $+10 \text{ V}$. (b) $G_{\text{on}} - \mu_{\text{FE}}$ plot of the 20 devices. $920 \text{ }^\circ\text{C}$ -7.5 sccm H_2 -14 kPa-28 v% methanol. (A colour version of this figure can be viewed online.)

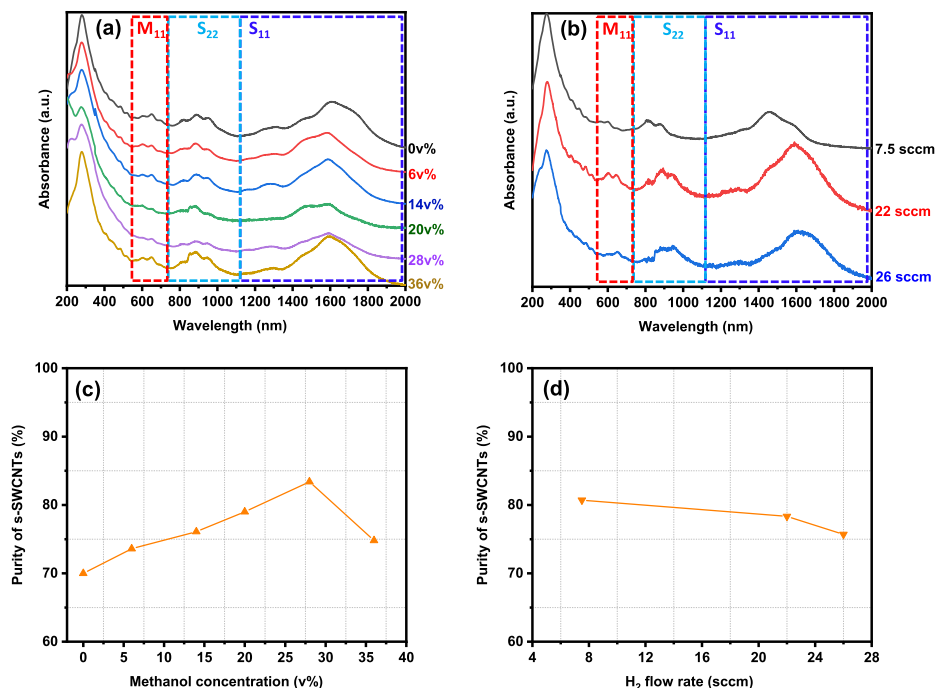


Fig. 4. Reproducibility study: The effects of methanol concentration and H₂ flow rate on s-SWCNT purity. (a) and (b) are optical absorption spectra. (c) and (d) are corresponding calculated purities of s-SWCNTs. Parameters for (a) and (c) are 940 °C-22 sccm H₂-0 kPa, for (b) and (d) are 940 °C-0 kPa-28 v%. (A colour version of this figure can be viewed online.)

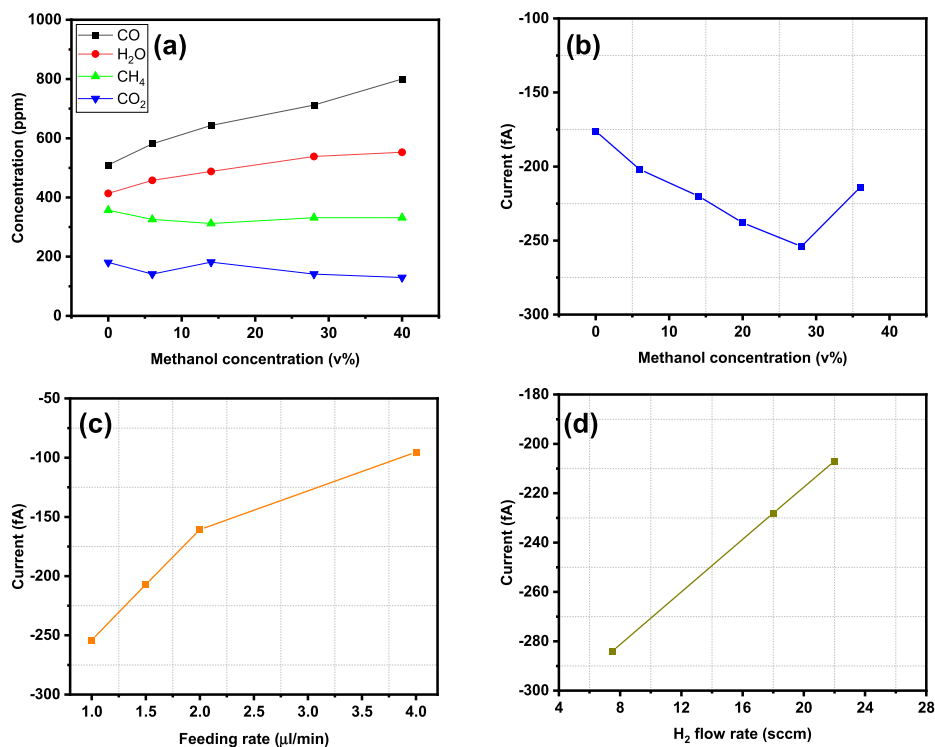


Fig. 5. Reproducibility study: Exploration of the origin of s-SWCNT enrichment with a gas-phase FT-IR spectrometer and an aerosol electrometer. (a) FT-IR results show the effect of methanol on the concentration of main decomposed products in the exhaust. 940 °C-22 sccm H₂-0 kPa. The effects of methanol concentration (b), feeding rate (c), and H₂ flow rate (d) on the net current of as-synthesized SWCNTs. Parameters for (a) and (b) are 940 °C-22 sccm H₂-0 kPa, for (c) and (d) are 940 °C-0 kPa-28 v%. (A colour version of this figure can be viewed online.)

current reaches the highest when the methanol concentration is 28 v% (Fig. 5b), which is consistent with the trend of s-SWCNT purity presented in Fig. 4c. But tuning the pressure leads to negligible variation in the net current, which matches with the slight

fluctuation in s-SWCNT purity (Figs. S22b and d). In addition, we investigated the effects of H₂ flow rate and feeding rate of precursors on the net current. The trends of net current agree well with the purity of s-SWCNTs in the two cases (Figs. 4d and 5c, d,

Fig. S23b). The results from the electrometer reveal that s-SWCNTs carry more negative charges and possibly grow faster than their metallic counterparts, providing an instant response to the optimization of growth parameters targeting high-purity s-SWCNTs. It was reported that the electronic density of state of s-SWCNT is larger compared with that of *m*-SWCNT when the catalyst particle is negatively charged, resulting in an increased number of electrons on the catalyst particle [49]. Therefore, the nucleation barrier of s-SWCNT is lower than that of *m*-SWCNT and s-SWCNT likely grows faster [50]. The variation of length (*i.e.*, growth speed) between s-SWCNT and *m*-SWCNT is currently under investigation. The effects of feeding rate (Fig. S23) and S/Fe ratio (Fig. S24) on the purity of s-SWCNTs were studied as well. Structure-controllable growth of SWCNTs is achieved usually by sacrificing the yield. We also observed that s-SWCNTs with higher purities yet lower yield are produced with a decreased feeding rate of precursors.

3.3. Discussion

We have found that there exists a parameter window where the s-SWCNTs with a purity close to 98% could be produced in a floating catalyst CVD reactor mainly by regulating the barometric pressure inside the quartz tube and the concentration of methanol added into the precursor solution. The breakthrough of continuous production of high-purity s-SWCNTs motivated us to repeat the experiments. Possible factors like the evaporation of thiophene, oxygen/moisture-remover capsule, quartz tube age, constant N₂ purging, *etc.* were all checked while the other growth parameters were kept constant. We also tried many other parameter combinations, but it turned out that only s-SWCNTs with moderate purities could be easily reproduced. Thus, we believe that the wall conditions of a quartz tube play a significant role in producing s-SWCNTs. An old quartz tube that has been run for two weeks improves the reproducibility of high-purity s-SWCNTs whereas a new one always produces s-SWCNTs with low purities. An old quartz tube was utilized for the synthesis of highly enriched s-SWCNTs. For three months, we have been producing s-SWCNTs with high purities displayed in Figs. 1 and 2. The importance of wall conditions in CNT synthesis has been addressed by others [51–53] as well. According to the absorption spectra (Figs. 1a and 2a, b) of the s-SWCNTs collected under the same growth parameters, a quartz tube saturated by carbon deposits and catalyst particles should be stable to produce s-SWCNTs with reasonable consistency.

Herein, we would like to call for the description (*e.g.*, detailed parameters, critical minutiae) of process reproducibility in the scientific community to benefit the reproducers. We recommend a few tips to improve data reproducibility for those who are working on the structure-controllable synthesis of SWCNTs:

- Preparing a new precursor solution for each run. Storing air, light, and/or moisture-sensitive chemicals by following the material safety data sheet.
- Purifying the carrier gas by removing residual oxygen and moisture with an oxygen/moisture trap installed after the outlet of a gas cylinder.
- Calibrating mass flow meters with a bubble meter at intervals suggested by the manufacturer.
- Use of the same quartz tube for a specific study to avoid cross-contamination.
- Recording the utilization duration of a quartz tube and checking the area of carbon coverage.
- Constantly purging the quartz tube with inert gas when no growth is carried on.
- Measuring the optical absorption spectrum of SWCNTs with a minimum air exposure time.

- Utilization of the data acquired only after stabilizing the reactor by comparing sequential optical absorption spectra.

4. Conclusions

In summary, we have demonstrated the feasibility of continuous production of semiconducting-enriched SWCNTs in an FCCVD reactor through increasing the barometric pressure inside the reactor and adding an appropriate volume of methanol. The barometric pressure and the methanol concentration were found to apparently tailor the purity of s-SWCNTs. The purity of s-SWCNTs collected under optimal conditions can reach 98% calculated from the absorption spectrum. Moreover, the mean diameter of SWCNTs is located in the range of 1.1–1.3 nm and the diameter distribution can be modulated by regulating methanol concentration and the flow rate of H₂. The mean bundle length of SWCNTs is 15.2 μm which is much longer than that of dispersion-sorted SWCNTs. We suggest that overpressure promotes the formation of specific carbon caps for the growth of high chiral angle s-SWCNTs. Additionally, an appropriate amount of methanol favors the growth of s-SWCNTs with the decomposed H₂O through selective etching unstable *m*-SWCNTs, reshaping catalyst nanoparticles, and suppressing the nucleation of *m*-SWCNTs, leading to the enrichment of s-SWCNTs with narrow diameter (*i.e.*, bandgap) distribution. FETs incorporating the as-collected s-SWCNTs exhibit excellent electrical performance. Although s-SWCNTs with a purity higher than 95% were hardly reproduced, our study points out a way to the large-scale production of s-SWCNTs for ultrahigh performance thin-film electronics with even energy landscape, particularly in the field of flexible and/or stretchable electronics.

CRediT authorship contribution statement

Er-Xiong Ding: Conceptualization, Methodology, Validation, Formal analysis, Investigation, Data curation, Writing, Visualization. **Peng Liu:** Methodology, Validation, Formal analysis, Investigation, Data curation, Writing, Visualization. **Abu Taher Khan:** Methodology, Validation, Formal analysis, Investigation, Data curation, Writing, Visualization. **Qiang Zhang:** Conceptualization, Validation, Formal analysis, Investigation, Data curation, Writing, Visualization, Project administration. **Nan Wei:** Methodology, Validation, Formal analysis, Investigation, Data curation, Writing, Visualization. **Hua Jiang:** Methodology, Validation, Formal analysis, Investigation, Data curation, Writing, Visualization. **Esko I. Kauppinen:** Conceptualization, Methodology, Validation, Formal analysis, Investigation, Data curation, Writing, Visualization, Project administration.

Declaration of competing interest

The authors declare that they have no known competing financial interests or personal relationships that could have appeared to influence the work reported in this paper.

Acknowledgment

This work was supported by the Academy of Finland via projects 286546 (DEMEC), 292600 (SUPER), and 316572 (CNTstress), as well as TEKES in Finland via projects 3303/31/2015 (CNT-PV) and 1882/31/2016 (FEDOC). P. Liu acknowledges the financial support from China Scholarship Council (No. 202006310007). This work made use of the Aalto University Nanomicroscopy Center (Aalto-NMC) premises. Aalto NanoFab (Micronova) cleanroom resources are greatly appreciated. The authors sincerely thank Dr. Mirkka Jones for proof reading.

Appendix A. Supplementary data

Supplementary data to this article can be found online at <https://doi.org/10.1016/j.carbon.2022.04.020>.

References

- Q. Zhang, N. Wei, P. Laiho, E.I. Kauppinen, Recent developments in single-walled carbon nanotube thin films fabricated by dry floating catalyst chemical vapor deposition, *Top. Curr. Chem.* 375 (2017) 1–30.
- L. Yu, C. Shearer, J. Shapter, Recent development of carbon nanotube transparent conductive films, *Chem. Rev.* 116 (2016) 13413–13453.
- Q. Zhang, W. Zhou, X. Xia, K. Li, N. Zhang, Y. Wang, Z. Xiao, Q. Fan, E.I. Kauppinen, S. Xie, Transparent and freestanding single-walled carbon nanotube films synthesized directly and continuously via a blown aerosol technique, *Adv. Mater.* 32 (2020) 1–8.
- J. Tang, Q. Cao, G. Tulevski, K.A. Jenkins, L. Nela, D.B. Farmer, S.J. Han, Flexible CMOS integrated circuits based on carbon nanotubes with sub-10 ns stage delays, *Nat. Electron.* 1 (2018) 191–196.
- A.D. Avery, B.H. Zhou, J. Lee, E.S. Lee, E.M. Miller, R. Ihly, D. Wesenberg, K.S. Mistry, S.L. Guillot, B.L. Zink, Y.H. Kim, J.L. Blackburn, A.J. Ferguson, Tailored semiconducting carbon nanotube networks with enhanced thermoelectric properties, *Nat. Energy* 1 (2016) 16033.
- R. Ihly, A.M. Dowgiallo, M. Yang, P. Schulz, N.J. Stanton, O.G. Reid, A.J. Ferguson, K. Zhu, J.J. Berry, J.L. Blackburn, Efficient charge extraction and slow recombination in organic-inorganic perovskites capped with semiconducting single-walled carbon nanotubes, *Energy Environ. Sci.* 9 (2016) 1439–1449.
- F. Hennrich, W. Li, R. Fischer, S. Lebedkin, R. Krupke, M.M. Kappes, Length-sorted, large-diameter, polyfluorene-wrapped semiconducting single-walled carbon nanotubes for high-density, short-channel transistors, *ACS Nano* 10 (2016) 1888–1895.
- N. Rouhi, D. Jain, P.J. Burke, High-performance semiconducting nanotube inks: progress and prospects, *ACS Nano* 5 (2011) 8471–8487.
- M.S. Arnold, A.A. Green, J.F. Hulvat, S.I. Stupp, M.C. Hersam, Sorting carbon nanotubes by electronic structure using density differentiation, *Nat. Nanotechnol.* 1 (2006) 60–65.
- G.S. Tulevski, A.D. Franklin, A. Afzali, High-purity isolation and quantification of semiconducting carbon nanotubes via column chromatography, *ACS Nano* 7 (2013) 2971–2976.
- J. Gu, J. Han, D. Liu, X. Yu, L. Kang, S. Qiu, H. Jin, H. Li, Q. Li, J. Zhang, Solution-processable high-purity semiconducting SWCNTs for large-area fabrication of high-performance thin-film transistors, *Small* 12 (2016) 4993–4999.
- Y. Che, C. Wang, J. Liu, B. Liu, X. Lin, J. Parker, C. Beasley, H.-S.P. Wong, C. Zhou, Selective synthesis and device applications of semiconducting single-walled carbon nanotubes using isopropyl alcohol as feedstock, *ACS Nano* 6 (2012) 7454–7462.
- W. Zhou, S. Zhan, L. Ding, J. Liu, General rules for selective growth of enriched semiconducting single walled carbon nanotubes with water vapor as in situ etchant, *J. Am. Chem. Soc.* 134 (2012) 14019–14026.
- A.E. Islam, J.A. Rogers, M.A. Alam, Recent progress in obtaining semiconducting single-walled carbon nanotubes for transistor applications, *Adv. Mater.* 27 (2015) 7908–7937.
- Q. Cao, S.J. Han, G.S. Tulevski, A.D. Franklin, W. Haensch, Evaluation of field-effect mobility and contact resistance of transistors that use solution-processed single-walled carbon nanotubes, *ACS Nano* 6 (2012) 6471–6477.
- T. Lei, L.-L. Shao, Y.-Q. Zheng, G. Pitner, G. Fang, C. Zhu, S. Li, R. Beausoleil, H.-S.P. Wong, T.-C. Huang, K.-T. Cheng, Z. Bao, Low-voltage high-performance flexible digital and analog circuits based on ultrahigh-purity semiconducting carbon nanotubes, *Nat. Commun.* 10 (2019) 2161.
- S. Qiu, K. Wu, B. Gao, L. Li, H. Jin, Q. Li, Solution-processing of high-purity semiconducting single-walled carbon nanotubes for electronics devices, *Adv. Mater.* 31 (2019) 1800750.
- S.H. Tseng, N.H. Tai, Fabrication of a transparent and flexible thin film transistor based on single-walled carbon nanotubes using the direct transfer method, *Appl. Phys. Lett.* 95 (2009) 204104.
- B. Yu, P.-X. Hou, F. Li, B. Liu, C. Liu, H.-M. Cheng, Selective removal of metallic single-walled carbon nanotubes by combined in situ and post-synthesis oxidation, *Carbon* 48 (2010) 2941–2947.
- B. Yu, C. Liu, P.-X. Hou, Y. Tian, S. Li, B. Liu, F. Li, E.I. Kauppinen, H.-M. Cheng, Bulk synthesis of large diameter semiconducting single-walled carbon nanotubes by oxygen-assisted floating catalyst chemical vapor deposition, *J. Am. Chem. Soc.* 133 (2011) 5232–5235.
- W.-S. Li, P.-X. Hou, C. Liu, D.-M. Sun, J. Yuan, S.-Y. Zhao, L.-C. Yin, H. Cong, H.-M. Cheng, High-quality, highly concentrated semiconducting single-wall carbon nanotubes for use in field effect transistors and biosensors, *ACS Nano* 7 (2013) 6831–6839.
- E.-X. Ding, H. Jiang, Q. Zhang, Y. Tian, P. Laiho, A. Hussain, Y. Liao, N. Wei, E.I. Kauppinen, Highly conductive and transparent single-walled carbon nanotube thin films from ethanol by floating catalyst chemical vapor deposition, *Nanoscale* 9 (2017) 17601–17609.
- L. Ding, A. Tselev, J. Wang, D. Yuan, H. Chu, T.P. McNicholas, Y. Li, J. Liu, Selective growth of well-aligned semiconducting single-walled carbon nanotubes, *Nano Lett.* 9 (2009) 800–805.
- Y. Tian, H. Jiang, J.v. Pfaler, Z. Zhu, A.G. Nasibulin, T. Nikitin, B. Aitchison, L. Khriachtchev, D.P. Brown, E.I. Kauppinen, Analysis of the size distribution of single-walled carbon nanotubes using optical absorption spectroscopy, *J. Phys. Chem. Lett.* 1 (2010) 1143–1148.
- P. Laiho, K. Mustonen, Y. Ohno, S. Maruyama, E.I. Kauppinen, Dry and direct deposition of aerosol-synthesized single-walled carbon nanotubes by thermophoresis, *ACS Appl. Mater. Interfaces* 9 (2017) 20738–20747.
- H. Jiang, A.G. Nasibulin, D.P. Brown, E.I. Kauppinen, Unambiguous atomic structural determination of single-walled carbon nanotubes by electron diffraction, *Carbon* 45 (2007) 662–667.
- N. Wei, P. Laiho, A.T. Khan, A. Hussain, A. Lyuleeva, S. Ahmed, Q. Zhang, Y. Liao, Y. Tian, E.-X. Ding, Y. Ohno, E.I. Kauppinen, Fast and ultraclean approach for measuring the transport properties of carbon nanotubes, *Adv. Funct. Mater.* 30 (2020) 1907150.
- B. Wang, L. Wei, L. Yao, L.J. Li, Y. Yang, Y. Chen, Pressure-induced single-walled carbon nanotube (n, m) selectivity on Co-Mo catalysts, *J. Phys. Chem. C* 111 (2007) 14612–14616.
- F. Zhang, P.-X. Hou, C. Liu, B.-W. Wang, H. Jiang, M.-L. Chen, D.-M. Sun, J.-C. Li, H.-T. Cong, E.I. Kauppinen, H.-M. Cheng, Growth of semiconducting single-walled carbon nanotubes with a narrow band-gap distribution, *Nat. Commun.* 7 (2016) 1–8.
- F. Yang, X. Wang, J. Si, X. Zhao, K. Qi, C. Jin, Z. Zhang, M. Li, D. Zhang, J. Yang, Z. Zhang, Z. Xu, L.-M. Peng, X. Bai, Y. Li, Water-assisted preparation of high-purity semiconducting (14,4) carbon nanotubes, *ACS Nano* 11 (2017) 186–193.
- S. Reich, L. Li, J. Robertson, Control the chirality of carbon nanotubes by epitaxial growth, *Chem. Phys. Lett.* 421 (2006) 469–472.
- V.I. Artyukhov, E.S. Penev, B.I. Yakobson, Why nanotubes grow chiral, *Nat. Commun.* 5 (2014) 4892.
- Y. Chen, D. Ciuparu, S. Lim, Y. Yang, G.L. Haller, L. Pfeifferle, Synthesis of uniform diameter single wall carbon nanotubes in Co-MCM-41: effects of CO pressure and reaction time, *J. Catal.* 226 (2004) 351–362.
- C. Liu, H.-M. Cheng, Controlled growth of semiconducting and metallic single-walled carbon nanotubes, *J. Am. Chem. Soc.* 138 (2016) 6690–6698.
- W. Zhou, L. Ding, S. Yang, J. Liu, Synthesis of high-density, large-diameter, and aligned single-walled carbon nanotubes by multiple-cycle growth methods, *ACS Nano* 5 (2011) 3849–3857.
- L. Kang, S. Zhang, Q. Li, J. Zhang, Growth of horizontal semiconducting SWNT arrays with density higher than 100 tubes/ μm using ethanol/methane chemical vapor deposition, *J. Am. Chem. Soc.* 138 (2016) 6727–6730.
- C.-M. Yang, K.H. An, J.S. Park, K.A. Park, S.C. Lim, S.H. Cho, Y.S. Lee, W. Park, C.Y. Park, Y.H. Lee, Preferential etching of metallic single-walled carbon nanotubes with small diameter by fluorine gas, *Phys. Rev. B* 73 (2006), 075419.
- V. Zolyomi, J. Kürti, First-principles calculations for the electronic band structures of small diametersingle-wall carbon nanotubes, *Phys. Rev. B* 70 (2004), 085403.
- A.R. Harutyunyan, G. Chen, T.M. Paronyan, E.M. Pigos, O.A. Kuznetsov, K. Hewaparakrama, S.M. Kim, D. Zakharov, E.A. Stach, G.U. Sumanasekera, Preferential growth of single-walled carbon nanotubes with metallic conductivity, *Science* 326 (2009) 116–120.
- A. Hussain, E.-X. Ding, B. Mclean, K. Mustonen, S. Ahmad, M. Tavakkoli, A.J. Page, Q. Zhang, J. Kotakoski, E.I. Kauppinen, Scalable growth of single-walled carbon nanotubes with a highly uniform structure, *Nanoscale* 12 (2020) 12263–12267.
- J.S. Barnard, C. Paukner, K.K. Koziol, The role of carbon precursor on carbon nanotube chirality in floating catalyst chemical vapour deposition, *Nanoscale* 8 (2016) 17262–17270.
- P.B. Amama, C.L. Pint, L. McJilton, S.M. Kim, E.A. Stach, P.T. Murray, R.H. Hauge, B. Maruyama, Role of water in super growth of single-walled carbon nanotube carpets, *Nano Lett.* 9 (2009) 44–49.
- Z. Zhu, N. Wei, W. Cheng, B. Shen, S. Sun, J. Gao, Q. Wen, R. Zhang, J. Xu, Y. Wang, F. Wei, Rate-selected growth of ultrapure semiconducting carbon nanotube arrays, *Nat. Commun.* 10 (2019) 4467.
- E.-X. Ding, Q. Zhang, N. Wei, A.T. Khan, E.I. Kauppinen, High-performance single-walled carbon nanotube transparent conducting film fabricated by using low feeding rate of ethanol solution, *R. Soc. Open Sci.* 5 (2018) 180392.
- P. Stokes, S.I. Khondaker, High quality solution processed carbon nanotube transistors assembled by dielectrophoresis, *Appl. Phys. Lett.* 96 (2010), 083110.
- Y. Liao, H. Jiang, N. Wei, P. Laiho, Q. Zhang, S.A. Khan, E.I. Kauppinen, Direct synthesis of colorful single-walled carbon nanotube thin films, *J. Am. Chem. Soc.* 140 (2018) 9797–9800.
- A. Li-Pook-Than, P. Finnie, Observation of the metallic-type selective etching of single walled carbon nanotubes by real-time in situ two-laser Raman spectroscopy, *Carbon* 89 (2015) 232–241.
- Z. Wang, Q. Zhao, L. Tong, J. Zhang, Investigation of etching behavior of single-walled carbon nanotubes using different etchants, *J. Phys. Chem. C* 121 (2017) 27655–27663.
- M.S. Dresselhaus, G. Dresselhaus, A. Jorio, A.G. Souza Filho, R. Saito, Raman spectroscopy on isolated single wall carbon nanotubes, *Carbon* 40 (2002) 2043–2061.
- J. Wang, X. Jin, Z. Liu, G. Yu, Q. Ji, H. Wei, J. Zhang, K. Zhang, D. Li, Z. Yuan, J. Li, P. Liu, Y. Wu, Y. Wei, J. Wang, Q. Li, L. Zhang, J. Kong, S. Fan, K. Jiang, Growing

- highly pure semiconducting carbon nanotubes by electrotwisting the helicity, *Nat. Catal.* 1 (2018) 326–331.
- [51] A.G. Nasibulin, P. Queipo, S.D. Shandakov, D.P. Brown, H. Jiang, P.V. Pikhitsa, O.V. Tolochko, E.I. Kauppinen, Studies on mechanism of single-walled carbon nanotube formation, *J. Nanosci. Nanotechnol.* 6 (2006) 1233–1246.
- [52] K. Liu, P. Liu, K. Jiang, S. Fan, Effect of carbon deposits on the reactor wall during the growth of multi-walled carbon nanotube arrays, *Carbon* 45 (2007) 2379–2387.
- [53] C.R. Oliver, E.S. Polsen, E.R. Meshot, S. Tawfick, S.J. Park, M. Bedewy, A.J. Hart, Statistical analysis of variation in laboratory growth of carbon nanotube forests and recommendations for improved consistency, *ACS Nano* 7 (2013) 3565–3580.